AGU PUBLICATIONS

Tectonics

RESEARCH ARTICLE
10.1002/2017TC004476

**Key Points:**
- Oblique active convergence across the Qilian Shan fold-and-thrust belt occurs by strain partitioning, similar to oblique subduction zones
- Interseismic crustal velocities are consistent with oblique motion on a single detachment thrust below 26 km depth
- Geomorphic and seismicity aspects of the Qilian Shan resemble a nascent orogenic plateau

**Supporting Information:**
- Supporting Information S1

**Correspondence to:**
M. B. Allen,
m.b.allen@durham.ac.uk

**Citation:**
Allen, M. B., R. J. Walters, S. Song, C. Saville, N. De Paola, J. Ford, Z. Hu, and W. Sun (2017), Partitioning of oblique convergence coupled to the fault locking behavior of fold-and-thrust belts: Evidence from the Qilian Shan, northeastern Tibetan Plateau, *Tectonics*, *36*, doi:10.1002/2017TC004476.

Received 13 JAN 2017
Accepted 26 JUL 2017
Accepted article online 10 AUG 2017



# Partitioning of oblique convergence coupled to the fault locking behavior of fold-and-thrust belts: Evidence from the Qilian Shan, northeastern Tibetan Plateau

**Mark B. Allen[1], Richard J. Walters[2], Shuguang Song[3], Christopher Saville[1], Nicola De Paola[1], Jonathan Ford[1], Zhenxing Hu[4], and Wenli Sun[4]**

[1]Department of Earth Sciences, University of Durham, Durham, UK, [2]COMET, Department of Earth Sciences, University of Durham, Durham, UK, [3]MOE Key Laboratory of Orogenic Belts and Crustal Evolution, School of Earth and Space Sciences, Peking University, Beijing, China, [4]School of Earth Sciences, Lanzhou University, Lanzhou, China

**Abstract** Oblique plate convergence is common, but it is not clear how the obliquity is achieved by continental fold-and-thrust belts. We address this problem in the Qilian Shan, northeastern Tibetan Plateau, using fieldwork observations, geomorphic analysis, and elastic dislocation modeling of published geodetic data. A thrust dips SSW from the northern range front and underlies steeper thrusts in the interior. Cenozoic thrust-related shortening across the Qilian Shan is ~155–175 km, based on two transects. Elastic dislocation modeling indicates that horizontal strain in the interseismic period is consistent with oblique slip on a single low-angle detachment thrust below ~26 km depth, dipping SSW at ~17°. We suggest that this detachment is located above North China Block crust, originally underthrust during Paleozoic orogeny. Horizontal shear strain is localized directly above the updip limit of creep on the detachment and is coincident with the left-lateral Haiyuan Fault. This configuration implies that oblique slip on the detachment below seismogenic depths is partitioned in the shallow crust onto separate strike-slip and thrust faults. This is consistent with strain partitioning in oceanic subduction zones but has not previously been found by dislocation models of continental interiors. The marginal, strike-slip, Altyn Tagh Fault influences thrusting within the Qilian Shan for 100–200 km from the fault but does not control the regional structure, where Paleozoic basement faults have been reactivated. The Qilian Shan resembles the main Tibetan Plateau in nascent form: active thrusts are marginal to an interior that is developing plateau characteristics, involving low relief, and low seismicity.

**Plain Language Summary** Tectonic plates commonly converge obliquely, meaning that the convergence direction is not head-on to the boundary between the two plates but slanted at an angle. This behavior is best known and understood from where an oceanic plate passes underneath another plate margin. The interiors of continents can also deform obliquely, but the deformation is not so well understood. In this study we have looked at the faults across a mountain range at the northeastern side of the Tibetan Plateau, the Qilian Shan, to understand how the oblique convergence takes place. Part of our work involves looking at the structures on the ground and through satellite imagery, and part reanalyses data previously gathered for the active rates of convergence across the range. The approaches give complementary results, in that the oblique convergence seems to be split into two components, one dipping under the range and one slicing along it. The data for the active slip place the range-parallel slicing above the point where the underlying, dipping, fault changes behavior, from earthquake-prone to earthquake-free. In this respect the Qilian Shan deforms remarkably simply, even though the continents are typically more complex than oceanic plates.

## 1. Introduction

A key question in continental tectonics is how overall plate convergence is accommodated within plate interiors. The India-Eurasia collision has been a natural focal point for debate, because of its size, total convergence, and active deformation rates [*Tapponnier and Molnar*, 1977; *Avouac and Tapponnier*, 1993; *Yin and Harrison*, 2000; *Tapponnier et al*., 2001; *England and Molnar*, 2005; *Thatcher*, 2007; *Royden et al*., 2008]. The Qilian Shan (Figures 1 and 2) has received particular attention because it currently deforms at rates of ~20% of the overall India-Eurasia convergence rate and is believed to be one of the youngest areas undergoing incorporation into the Tibetan Plateau [*Meyer et al*., 1998; *Zhang et al*., 2004; *Yin et al*., 2008a; *Duvall et al*., 2013; *Yuan et al*., 2013;

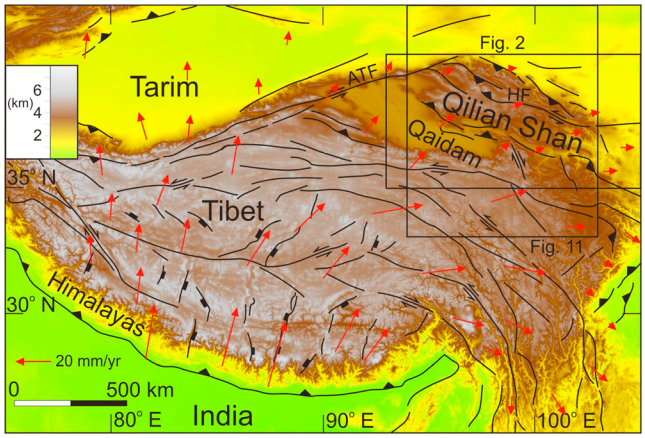


**Figure 1.** Summary of structures of the India-Eurasia collision, simplified from *Taylor and Yin* [2009], with GPS velocities in a stable Eurasia frame, selected from *Liang et al.* [2013].

*Zuza et al.*, 2016]. It is also an example of oblique convergence during continental collision (Figure 1) [*Gaudemer et al.*, 1995; *Zheng et al.*, 2013a; *Daout et al.*, 2016], where the strain is separated (partitioned) into dip-slip and strike-slip components (Figure 2). Such zones are to be expected: ~45% of active plate boundary convergence is distinctly oblique (>22% from the normal direction to the boundary) [*Woodcock*, 1986]. However, it is not clear how the strain partitioning operates within individual fold-and-thrust belts. For example, what controls the location of the faults that achieve the strike-slip component of the deformation?

This paper is an integrated study of the processes of oblique convergence in the Qilian Shan, based on results from fieldwork and remote sensing data, analysis of the regional topography and seismicity, and elastic dislocation modeling of published geodetic data. In particular, we investigate how strain partitioning takes place in a region previously proposed to be underlain by a regional low-angle thrust (Figure 3) [*Burchfiel et al.*, 1989; *Tapponnier et al.*, 1990; *Meyer et al.*, 1998; *Yin et al.*, 2008b; *Guillot and Replumaz*, 2013] and aim to understand how the strike-slip component of such partitioning is located within the fold-and-thrust belt.

Fieldwork in 2013 and 2014 focused on the completion of transects across the northern half of the Qilian Shan, supplemented by more reconnaissance level observations of range front geology at the southern and western sides of the region. These observations are coupled with existing 1:200,000 geological maps and satellite imagery from Google Earth to construct two regional cross sections, at a scale of ~1:200,000, ~150 km long in total. These cross sections help understand the location and style of deformation at present exposure levels and help constrain the overall structure and amount of shortening. There was also focus on the evidence, or lack of it, for Quaternary and Holocene deformation in different areas.

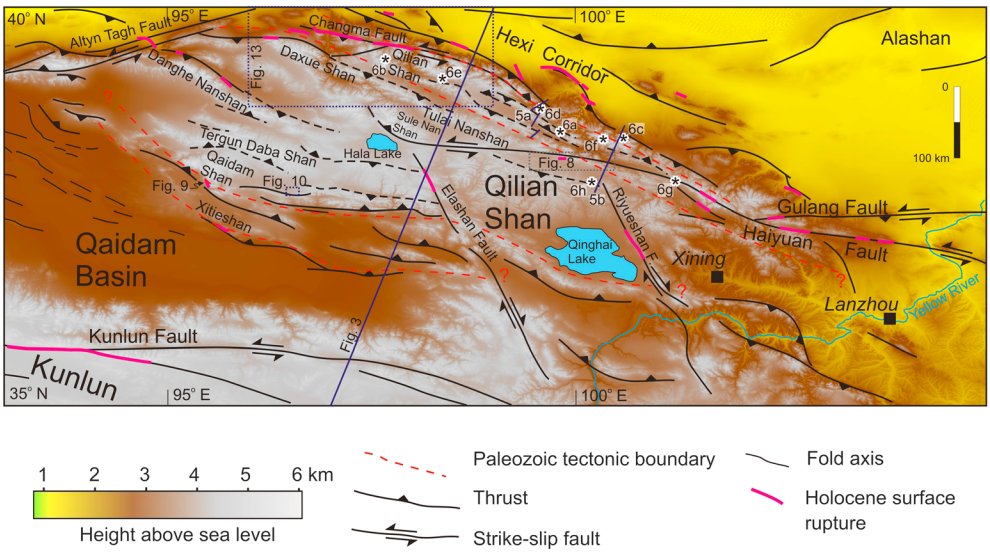


**Figure 2.** Major late Cenozoic structures of the Qilian Shan and Qaidam Basin, modified from *Taylor and Yin* [2009], with Hexi Corridor details from *Zheng et al.* [2013b]. Earthquake surface ruptures are derived from *Tapponnier et al.* [1990], *Gaudemer et al.* [1995], *Meyer et al.* [1998], *Washburn et al.* [2001], *Van der Woerd et al.* [2001], *Xu et al.* [2010], *Chen et al.* [2013], and this study.

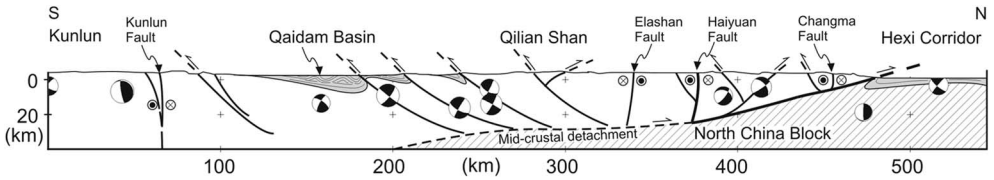


**Figure 3.** Interpretation of the deep structure of the Qilian Shan as detached on a regional low angle thrust, following *Burchfiel et al*. [1989] and *Meyer et al*. [1998]. Thrusts are shown as listric, and flattening onto the detachment, although this is not evident from the focal mechanisms (selected from representative data shown on Figure 4a). The bold lines indicate locked fault segments, from elastic dislocation modeling; see text for discussion. The basins are shown by grey shade. The line of section is shown in Figure 2.

We have used available GPS data (Global Earthquake Model (GEM) Strain Rate Model compilation [*Kreemer et al*., 2014, and references therein]) and simple elastic models to test whether the observed range-normal and range-parallel velocities for the Qilian Shan are consistent with interseismic strain accumulation across two shallowly locked, localized faults: a detachment thrust and strike-slip fault, respectively. This approach is a quantitative test of existing models that propose the existence of an active regional detachment thrust below the Qilian Shan [*Meyer et al*., 1998; *Yin et al*., 2008b; *Daout et al*., 2016] and also allows us to investigate the geometric relationship between strike-slip and dip-slip faulting within the range.

We have analyzed Shuttle Radar Topography Mission (SRTM) digital elevation data (http://www2.jpl.nasa.gov/srtm/; http://srtm.csi.cgiar.org) to gain insights from the regional topography on the present regional structure and in particular to understand the role of the strike-slip Altyn Tagh Fault in controlling the thrust structure of the Qilian Shan; this is potentially another aspect of the oblique convergence across the range [*Meyer et al*., 1998].

## 2. Regional Background

### 2.1. Structure

The Qilian Shan (shan = mountains) consists of a series of subparallel mountain ranges, separated from the main part of the Tibetan Plateau by the Qaidam Basin. Each subrange within the Qilian Shan is typically tens of kilometers across and hundreds of kilometers long (Figure 2). The name Qilian Shan is applied to the whole region between the Qaidam Basin and the discontinuous basins of the Hexi Corridor to its north, but also specifically to the northernmost of these individual ranges, and to a single peak. Present summit elevations across the Qilian Shan region are commonly >5000 m above sea level, with valley floors at ~2000–4000 m. Individual ranges are usually bounded by Cenozoic thrusts [*Tapponnier et al*., 1990; *Meyer et al*., 1998; *Van der Woerd et al*., 2001].

Present crustal thicknesses reach ~60–70 km in the Qilian Shan, contrasting with ~55 km for the interior of the Qaidam Basin and 45–50 km for the Tarim Basin and Hexi corridor to the northwest and north of the Qilian Shan [*Wang et al*., 2013; *Tian and Zhang*, 2013; *Feng et al*., 2014].

Basement of the Qilian Shan consists largely of rocks which formed in arcs and accretionary complexes, as well as an ultrahigh pressure metamorphic belt. These units collectively underwent a long evolution of oceanic subduction through to continental collision between the Qaidam Block and the Alashan (western part of the cratonic North China Block), from ~520 to 400 Ma [*Gehrels et al*., 2003; *Xiao et al*., 2009; *Song et al*., 2013, 2014; *Wu et al*., 2016]. There is also Proterozoic basement, both within the Qilian Shan, and probably underlying the Qaidam Basin [*Lu*, 2002; *Xu et al*., 2015]. The central part of the Qilian Shan is underlain by Proterozoic basement and sedimentary cover and is known as the Qilian Block; the more juvenile, accretionary crust to its north is grouped as the North Qilian Orogen. Collision between the Qilian Block and the arc/accretionary material of the North Qilian Orogen took place in the Early Paleozoic [*Song et al*., 2013]. Paleozoic tectonic boundaries trend WNW-ENE, parallel to the present structural and geomorphic grain of the Qilian Shan (Figure 2). Precambrian basement of the North China Block (Alashan) lies to the north of the Qilian Shan, underlying Mesozoic basins strung out along the Hexi Corridor [*Vincent and Allen*, 1999].

Carboniferous and Permian rocks in the Qilian Shan include both marine and nonmarine successions, indicating that the region was close to sea level at this time [e.g., *Wang and Yu*, 1995]. Carboniferous strata include

coal measures [*Geological Bureau of Qinghai Province*, 1968a]. Mesozoic strata are typically nonmarine [*Vincent and Allen*, 1999; *Horton et al*., 2004], including Triassic fluvial strata and Jurassic coal measures typical of other parts of northern China. Cretaceous sandstones are fluvial red beds, marking more arid conditions. Cenozoic strata are broadly similar to the Cretaceous rocks.

Cenozoic deformation and consequent exhumation may have begun as early as the Eocene, i.e., not long after initial India-Eurasia collision [*Clark et al*., 2010; *Zhuang et al*., 2011], but rates accelerated and wider areas were affected by ~15 Ma or later [*Palumbo et al*., 2009; *Zheng et al*., 2010; *Lease et al*., 2011; *Zhang et al*., 2012; *Duvall et al*., 2013; *Yuan et al*., 2013; *Liu et al*., 2017]. Such a history does not suggest a smooth outward progression to the growth of the Tibetan Plateau over time, but it is broadly consistent with the northeastern part of the plateau being relatively young [*Tapponnier et al*., 2001; *Yuan et al*., 2013].

Late Cenozoic and active faults are shown in Figure 2, adapted from *Taylor and Yin* [2009]. Thrusts typically lie at the foot of and parallel to the major ranges that form the Qilian Shan and trend ~WNW-ESE. There are up to seven main ranges, which have more individual expression in the wider, western part of the region (Figure 2). From north to south these are the Qilian Shan (in the narrow sense), Daxue Shan-Tulai Nanashan, Sule Nanshan, Danghe Nanshan, Tergun Daba Shan, Qaidam Shan, and a lower elevation, discontinuous series of ridges along the northern margin of the Qaidam Basin (e.g., the Xitieshan).

Two main left-lateral strike-slip faults form first-order elements in the geology of the study area (Figures 1 and 2). The Altyn Tagh Fault trends at N250°W and forms the northern margin to the Qilian Shan. The active and Holocene slip rate is ~10 mm $yr^{-1}$ and decreases to the ENE, based on both GPS data and offsets of geomorphic features [*Zhang et al*., 2004; *Cowgill et al*., 2009]. Total offset has been estimated at ~350 km by several groups [e.g., *Zhang et al*., 2001]. Thickening of the crust within the Qilian Shan has been interpreted as coupled to propagation of this fault, in a giant "horsetail" splay [*Meyer et al*., 1998].

The Haiyuan Fault runs for ~850 km at N110°E, through the central and eastern Qilian Shan and eastward (Figure 2), and is proposed as the main strike-slip component of overall strain partitioning [*Gaudemer et al*., 1995]. Active slip rate estimates from GPS and interferometric synthetic aperture radar (InSAR) are in agreement at 4–6 mm $yr^{-1}$, [*Zhang et al*., 2004; *Cavalie et al*., 2008; *Jolivet et al*., 2012; *Zheng et al*., 2013a]. Estimates for the total offset vary widely, from 10 to 95 km, based on displaced geological and geomorphic markers [*Burchfiel et al*., 1991; *Gaudemer et al*., 1995; *Ding et al*., 2004]. The western end of the Haiyuan Fault occurs where it bends northward into the Sule Nanshan range (Figure 2); this region includes the single highest peak in the Qilian Shan, Kangze'Gyai (>5800 m).

Other strike-slip faults cutting the Qilian Shan and adjacent areas to the south are the right-lateral Elashan and Riyueshan faults (Figure 2), described as having ~10 km of offset each, and likely to be moving at ~1 mm $yr^{-1}$ since ~10 Ma [*Yuan et al*., 2011].

### 2.2. Seismicity

Several $M > 7$ earthquakes have affected the area in historic times (Figure 4a). These events include the 1927 Gulang event, which killed ~40,000 people, and, just to the east of the area covered in Figure 4a, the 1920 Haiyuan earthquake, which killed >200,000 [*Gaudemer et al*., 1995]. These large events are concentrated on the northern side of the Qilian Shan and adjacent Hexi Corridor [*Xu et al*., 2010]; *Lee et al*. [1976] noted that the historical earthquake record may have a recording bias toward these areas, because of their relatively high population density.

Figure 4a shows focal mechanisms for the study area, derived from a combination of body wave modeling [*Molnar and Lyon-caen*, 1989; *Chen et al*., 1999; *Elliott et al*., 2010] and from the Global Centroid Moment Tensor (CMT) catalog (http://www.globalcmt.org). Thrust events are concentrated at lower elevations around the margins of the Qilian Shan but are scarce in the range interior. Low-angle events (<30° dip) are rare (Figure 4b). Clusters of earthquakes occurred in 2008 and 2009 at the southern side of the Qilian Shan (Figure 4a), which, along with other events, make this an unusually high seismicity area [*Elliott et al*., 2011; *Chen et al*., 2013]. While most of these events are thrusts, three are strike-slip events and are discussed in section 3.1.2. Earthquakes with $M > 4$ are also shown on Figure 4a, from the National Earthquake Information Center (NEIC) catalog (http://earthquake.usgs.gov/earthquakes/search/), and quoted with epicenter determinations typically of a few tenths of a degree, i.e., several tens of kilometers.

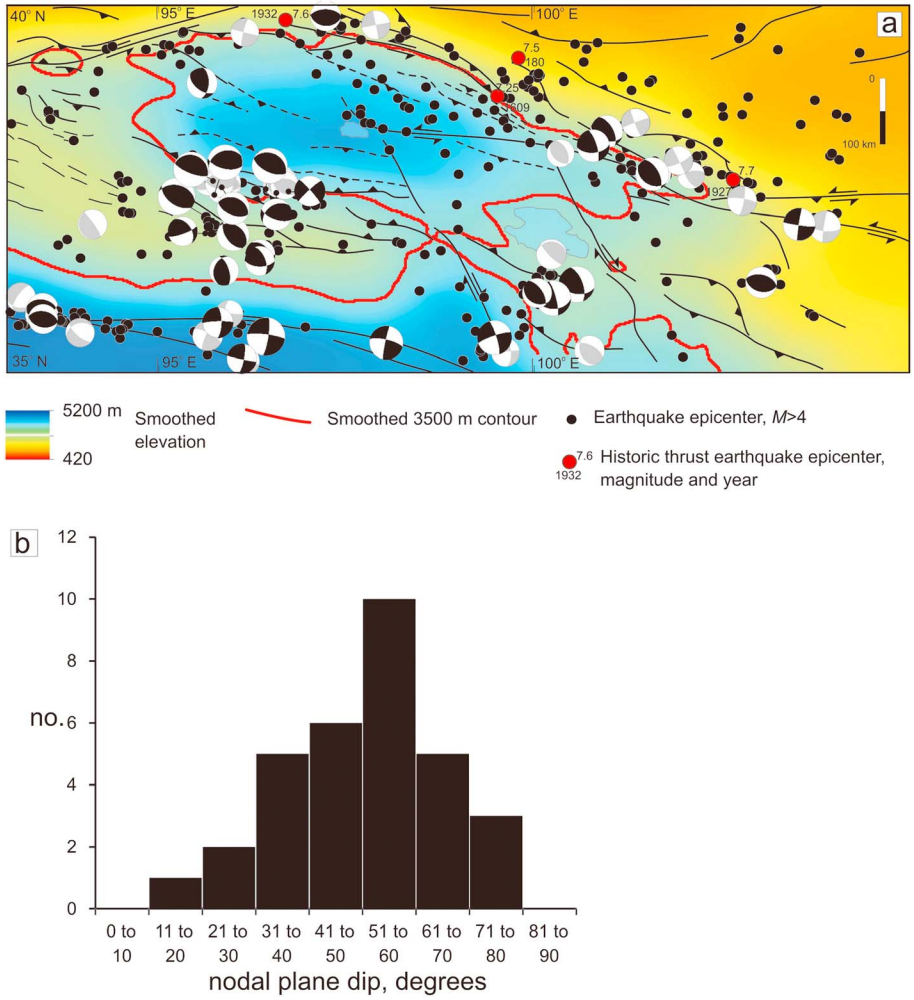


**Figure 4.** (a) Seismicity of the Qilian Shan, Qaidam Basin, and adjacent regions. The black focal mechanisms are from body wave modeling [*Molnar and Lyon-caen*, 1989; *Elliott et al.*, 2010] or the Global CMT catalog where $M > 5.3$ and there is >70% double couple. The grey focal mechanisms are from the Global CMT catalog where $M < 5.3$ and/or there is <70% double couple. See Tables S1 and S2. Epicenters of $M > 4$ events are from the NEIC catalog; historic thrust epicenters are from *Xu et al.* [2010]. Regional topography is smoothed over a 75 km radius moving window from SRTM data. (b) Histogram of thrust focal mechanism dip angles from the Qilian Shan, taken from sources listed for Figure 4a.

Several of the largest historic earthquakes produced surface ruptures which have been studied in the field [*Peltzer et al.*, 1988; *Tapponnier et al.*, 1990; *Gaudemer et al.*, 1995; *Meyer et al.*, 1998; *Hetzel et al.*, 2004; *Champagnac et al.*, 2010; *Xu et al.*, 2010]. These are concentrated at the margins of the Qilian Shan, especially at the edge of the Hexi Corridor on its northern side, but also in the west, typically within ~100 km of the Altyn Tagh Fault (Figures 2 and 4a). Most of these events are associated with thrust faulting, but strike-slip events have been recorded, and even an oblique normal rupture associated with the 1954 Shandan earthquake in the Hexi Corridor [*Xu et al.*, 2010].

## 3. Observations

### 3.1. Structure From Fieldwork and Remote Sensing Analysis

New observations in this section add to our understanding of the distribution of strain across the Qilian Shan and the relationship of the late Cenozoic deformation to the older structures and stratigraphy in the region.

#### 3.1.1. Contractional Deformation

Figure 5 shows two NNE-SSW cross sections for the northern part of the Qilian Shan, centered around ~99.5°E and 100.5°E, i.e., >100 km east of sections presented in *Meyer et al.* [1998] and *Şengör and Okurogullari* [1991].

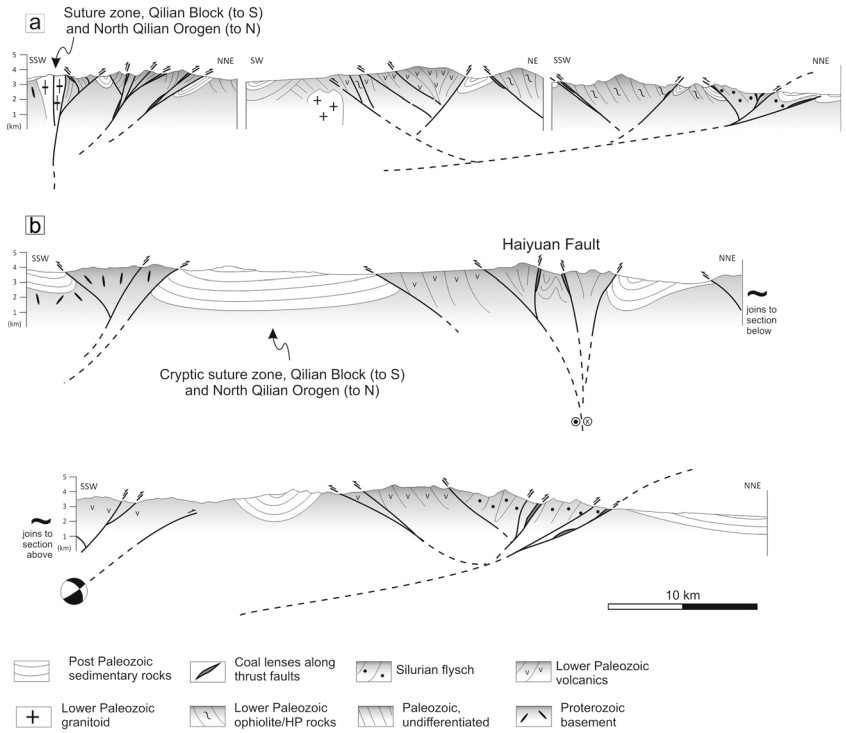


**Figure 5.** Cross sections through the northern Qilian Shan, based on original fieldwork and data from *Geological Bureau of Qinghai Province* [1968a, 1968b, 1980]. Location shown in Figure 2.

Lower Paleozoic rocks are a mixture of metasediments, volcanics, granitoids, ophiolitic assemblages (e.g., gabbro and serpentinite), and high-pressure metamorphic rocks [*Song et al*., 2013]. These lithologies are typically foliated and/or intensely folded (Figure 6a), which is absent from overlying Carboniferous and younger sedimentary rocks at present exposure levels, and so constrains the Early Paleozoic age of the penetrative fabrics. Proterozoic basement and a mixed carbonate-clastic Upper Proterozoic sedimentary cover crop out in the southern part of the area covered by the section line. The valley north of these Proterozoic rocks marks the suture between the Qilian Block and the North Qilian Orogen [*Song et al*., 2013] (Figure 5b).

Many of the regional valleys between the prominent, linear, ridges of Paleozoic/Precambrian outcrops are large-scale synclines of Triassic-Cenozoic strata, overthrust from one or both margins (Figure 6b). There is a strong correspondence between the traces of major Paleozoic structural boundaries and the location of the main Cenozoic thrust faults (Figure 2) [*Taylor and Yin*, 2009; *Song et al*., 2013; *Wu et al*., 2016].

The northernmost range front represents a major thrust boundary, displacing the Qilian Shan over the Hexi Corridor to the north [*Zuza et al*., 2016]. Thrust planes exposed within 5 km of the range front typically dip at $\leq$35° (Figure 6c), which is a lower angle than the thrusts to the south. The mountain front is not linear but contains salients and reentrants up to 15 km across [*Geological Bureau of Qinghai Province*, 1968a] suggesting low-angle thrusting.

Within the sections of Figure 5, to the south of the northern marginal thrust, there is no consistent structural vergence: thrust dip, structural relief, and the degree of folding in the synclines are roughly equal on the north and south facing range fronts. There is no large-scale imbrication of the Triassic-Cenozoic strata or structural windows or klippen that would indicate large-scale horizontal transport of thrust sheets on Alpine or Himalayan scales (i.e., many tens of kilometers).

The presence of folded and faulted Cretaceous and Tertiary strata, within the synclines and in the footwalls of the major thrusts, indicates the Cenozoic age of brittle thrusting. A data set of these brittle thrust faults, recorded predominantly along the transects of Figure 5, has an average strike of 291° and dip of 41° (Figure 7). This average is of similar strike but lower dip than Paleozoic foliations in the same localities

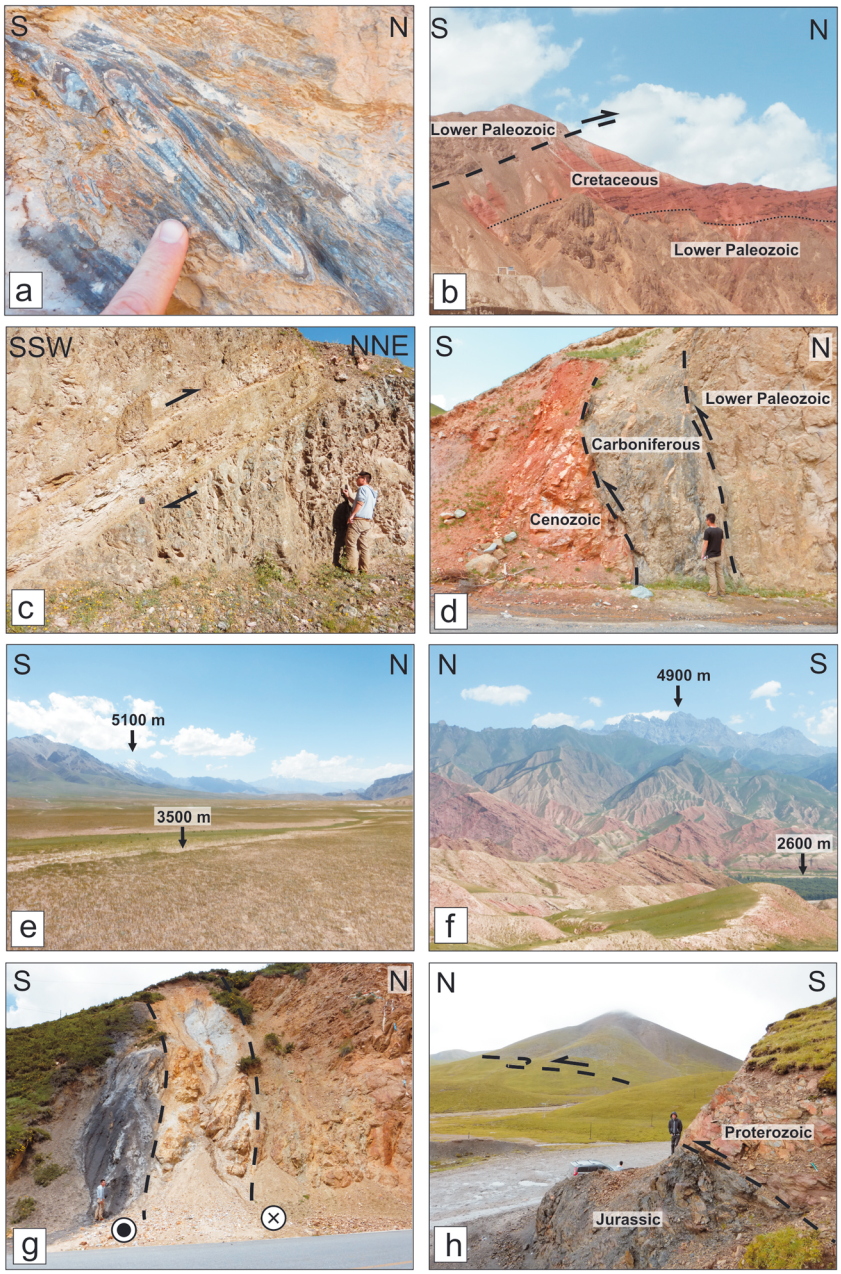


**Figure 6.** Field photographs of Qilian Shan structures and landscapes, located in Figure 2: (a) isoclinal folds in Lower Paleozoic blueschists; (b) brittle thrust placing Paleozoic basement rocks over Cretaceous strata; (c) brittle thrust with cataclasite breccia, within Ordovician volcanics at the northern margin of the Qilian Shan; (d) thrusted Lower Paleozoic and Cenozoic strata, with an intervening smear of Carboniferous coal-bearing shales; (e) typical landscape within the interior of the Qilian Shan, showing the relatively low relief; (f) higher relief of the Qilian Shan at its northern range front; (g) fault-bound slivers within the Haiyuan Fault; and (h) thrust at the northwestern end of the Riyueshan Fault.

(295°; 77°). Foliation data from the Xitieshan area of the southern range margin of the Qilian Shan have a distinctly different mean orientation of 345°/88°E (Figure 7).

Coal-bearing strata are commonly exposed in slivers along the fault planes, such that these rocks appear to lubricate many of the major thrusts (Figures 5 and 6d). These slivers are mapped as Carboniferous in age, consistent with the coal seams of that age in the region, but it is possible that some are Jurassic, given that Jurassic strata are also coal-bearing, albeit more restricted in their distribution. Fault gouge and cataclasite breccia are common, but there are not exposures of ductile shear zone lithologies such as mylonite.

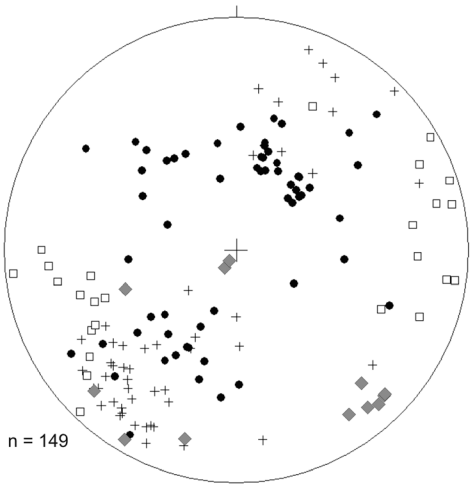


Circles - poles to brittle thrust planes; Crosses - poles to Paleozoic foliations; Squares - poles to Paleozoic foliations from the UHP belt, Xitieshan; Diamonds - slickenlines from the Haiyuan Fault.

**Figure 7.** Stereoplot of structural data from the Qilian Shan illustrating the variation between thrust planes of assumed Cenozoic age and penetrative fabrics within Paleozoic rocks. Foliations in the Xitieshan region at the southern side of the Qilian Shan (Figure 2) have a more north-south orientation than elsewhere. Haiyuan Fault slickenlines are predominantly low plunge, supporting strike-slip motion, but a subset indicates dip slip. Haiyuan Fault data are from localities shown in Figures 8 and 6b.

Although many range fronts are linear and sharp, there is a lack of unequivocal evidence for active thrusting along the range interiors, in contrast to the main north and south range fronts of the Qilian Shan, where active thrusting is well documented, albeit in discontinuous segments [*Tapponnier et al*., 1990; *Meyer et al*., 1998; *Hetzel et al*., 2004; *Yin et al*., 2008a; *Xu et al*., 2010; *Chen et al*., 2013].

The majority of thrusts in the south of the Qilian Shan are directed southward, toward the interior of the Qaidam Basin (Figure 3) [see also *Yin et al*., 2008a]. Combined with the northward thrusting at the northern margin of the range, noted above, this produces an overall divergence to the pattern of thrust transport, resembling a large-scale version of the individual thrusted ridges shown in Figure 5.

Triassic-Cenozoic basin fill is typically ≥3 km thick in the intermontane basins [e.g., *Geological Bureau of Qinghai Province*, 1968a]. Range crests are presently ~1–2 km above the valley floors within the Qilian Shan (Figures 6e and 6f). These values give a rough estimate of the minimum thrust throw at each range front of ~5 km, using an assumption that the exposed Lower Paleozoic basement was below the level of the basal Triassic rocks at the start of Cenozoic deformation. Mesozoic deformation cannot be discounted, so that not all the throw is definitely Cenozoic in age. However, although there are local unconformities within the Mesozoic section, there is no evidence of shortening and deformation on the magnitude of the Cenozoic tectonics. Folding of Mesozoic and Cenozoic strata indicates strain within the intermontane basins, although not on the scale of the thrusted ranges. Typical shortening across each of these basins in Figure 5 is on the order of 10–15%, derived by simple unfolding of the projected basal unconformity for each basin. We estimate regional shortening in section 4.

#### 3.1.2. Strike-Slip Deformation

We examined the Haiyuan Fault between 99.5° and 100.5°E, in a region further west than previous studies of this structure. The fault in this region includes an eastern segment which trends subparallel to the Paleozoic basement grain, passing westward into a segment at ~100.2°E, which cuts obliquely across the basement and folded Mesozoic rocks (Figure 8a). The fault zone contains anastomosing lenses of contrasting lithologies, at varying scales upward from meter-sized lozenges (Figure 6g) to kilometer-scale slivers. Weak lithologies such as shale, coal, and serpentinite are common, deformed by intense brittle fault networks. Subhorizontal slickenlines are common within the Haiyuan Fault but rare along other major structures shown within Figure 5. Even within the Haiyuan Fault there are dip-slip slickenlines, indicating thrust motion (Figure 7). We cannot discount that at least some of these dip-slip structures relate to pre-Cenozoic deformation, but as noted, Paleozoic rocks are typically deformed with penetrative fabrics not seen in the post-Paleozoic section. The width of the entire Haiyuan Fault zone is ~10 km in this region, based on the presence of subvertical faults with subhorizontal slip across this distance.

Offset bedrock geology can be matched across the Haiyuan Fault in the region of 100°E, i.e., where the fault cuts across the Paleozoic grain and further west than the locations of most of the previous offset estimates [*Burchfiel et al*., 1991; *Gaudemer et al*., 1995; *Ding et al*., 2004]. Paleozoic and Mesozoic rock units and the faults that separate them are offset for ~10 km (Figure 8a), based on 1:200,000 survey mapping [*Geological Bureau of Qinghai Province*, 1968a, 1968b]. We confirmed the left-lateral slip sense and vertical orientation of this fault

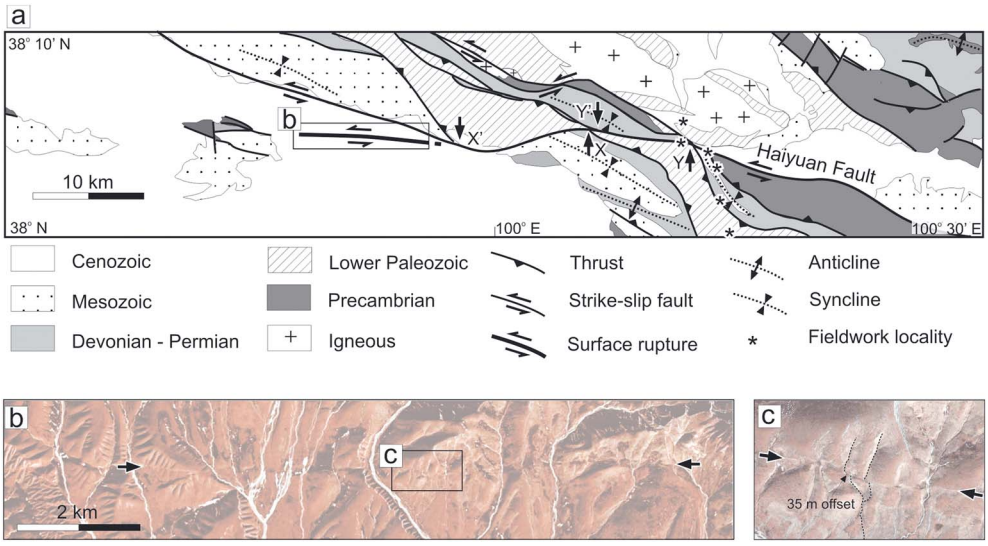


**Figure 8.** (a) Structure of the Haiyuan Fault at ~100°E [*Geological Bureau of Qinghai Province*, 1968a, 1968b]; (b) surface rupture across Quaternary sediments, located in Figure 8a; and (c) close-up of ruptures in Figure 8b. Quickbird satellite imagery from Google Earth (©2014 Google, ©2014 DigitalGlobe).

where it juxtaposes ophiolitic mélange against Permian strata (Figure 8a). This offset is distinctly lower than most previous estimates for the Haiyuan Fault (which are up to 95 km [*Gaudemer et al*., 1995]), based on a variety of approaches from bedrock offset, to the apparent left-lateral offset of the Yellow River (Figure 2). The difference between our estimate and most previous studies suggests that Figure 8a shows only part of the total offset, with major but unquantified slip occurring on other fault strands to the north and south, examined during our fieldwork (Figure 8a). An alternative but complementary explanation for our relatively low offset estimate is that there is an along-strike gradient in slip, decreasing westward toward the end of the Haiyuan Fault in the Sule Nan Shan (Figure 2).

Offset is harder to determine where the Haiyuan Fault is parallel to the regional bedrock structure. On the regional scale, the Haiyuan Fault also crosses the Paleozoic structural grain of the Qilian Shan at a low angle of obliquity and from east to west passes into the interior of the range from its northern margin (Figure 2). The segments parallel to the basement fabric are effectively right-stepping restraining bends and have been associated with thrust earthquakes (Figure 4a). This is a possible explanation for the more steeply plunging, dip-slip slickenlines within the broad fault zone (Figure 7).

Figure 8b shows a previously unreported trace of a segment of the Haiyuan Fault, where it cuts the Quaternary sediments of an intermontane basin for a length of ~12 km. The segment trends east-west and continues from the western end of the strand described above at 100°E. Individual stream gullies are offset left-laterally by ~35 m (Figure 8c), suggesting that this offset represents cumulative Quaternary displacement over an unknown number of earthquakes, rather than a single rupture.

We report another previously unidentified surface rupture at the southern margin of the Qilian Shan, near the Xitieshan Fault, on the Qaidam Thrust [*Yin et al*., 2008b] (Figure 9). Here there is a linear, sharp scarp in the surface of the alluvial fans. The rupture can be traced for ~8 km across the piedmont (Figures 9a and 9b), consistent with a $M \sim 6$ Holocene earthquake in this area [*Wells and Coppersmith*, 1994]. The slip sense is not clear and needs further work (access was not possible during our fieldwork). The regional elevation of the adjacent range to the northeast argues for a thrust component. A strike-slip or oblique sense is possible; faint rupture patterns in the imagery suggest a right-lateral component (Figure 9c), which would be consistent to the right-lateral slip observed to the east on the Elashan and Riyueshan faults (Figure 2).

A fault trending northwest-southeast, east of Xitieshan, is visible in satellite imagery (Figure 10) but does not appear to have been mapped previously [*Geological Bureau of Qinghai Province*, 1968a, 1968b]. Offset sense is right-lateral, and the fault is parallel to the much larger and more prominent Elashan and Riyueshan faults to the east (Figure 2). The faulting east of Xitieshan may represent a less developed

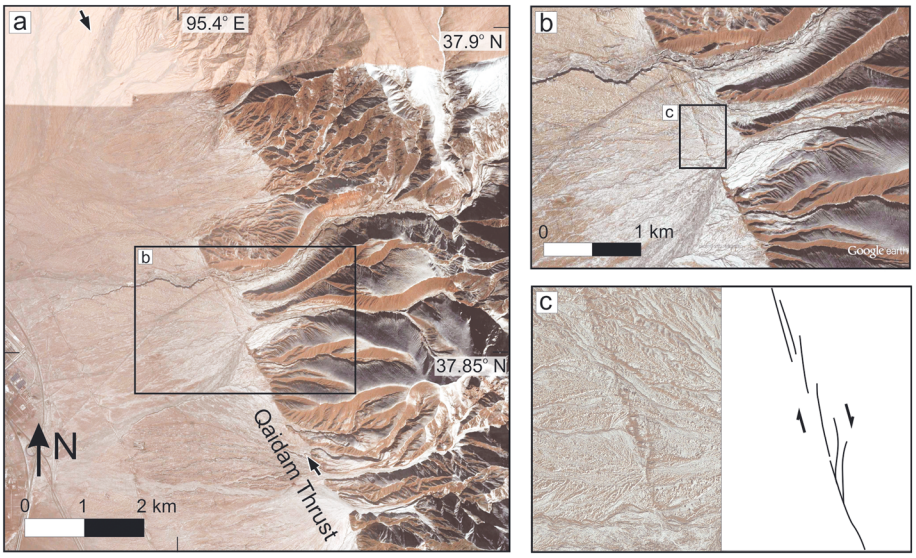


**Figure 9.** Quickbird satellite imagery from Google Earth (©2014 Google, ©2014 DigitalGlobe) of the Chaidanzhen fault break on the Qaidam Thrust. Location shown on Figure 2.

equivalent of the Elashan and Riyueshan faults, which were interpreted by *Duvall and Clark* [2010], *Yuan et al*. [2011], and *Zuza and Yin* [2016] to help accommodate shortening by counterclockwise rotation. Three strike-slip earthquake focal mechanisms corroborate the fault slip sense and show it to be an active structure (Figure 10e).

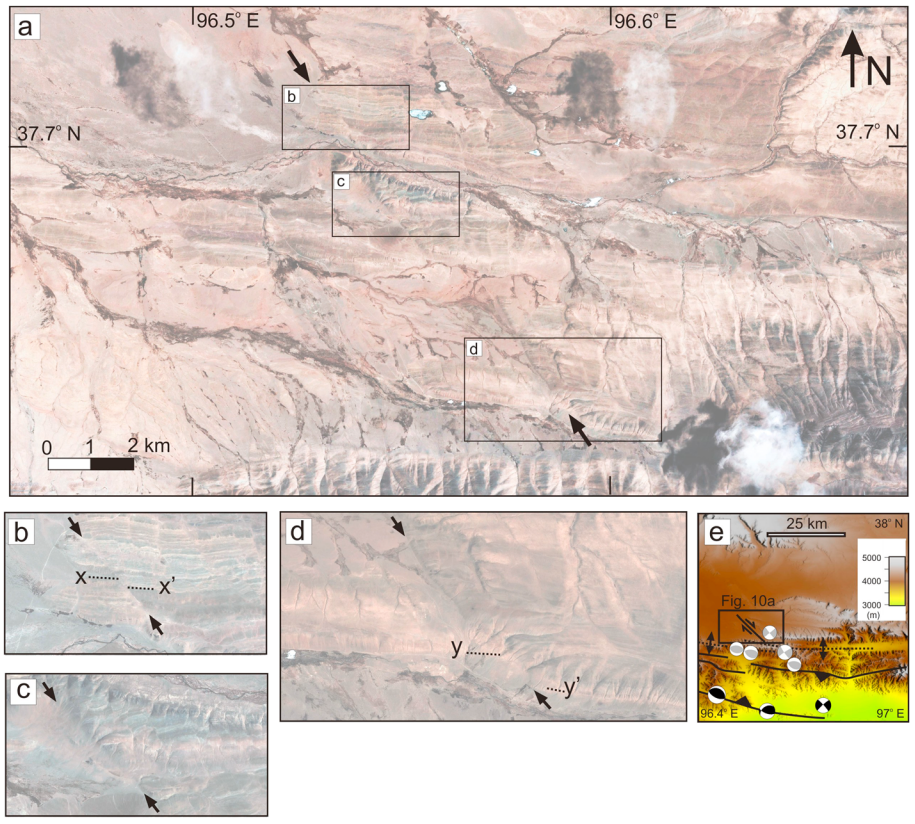


**Figure 10.** (a–d) Quickbird satellite imagery from Google Earth (©2014 Google, ©2014 DigitalGlobe) showing right-lateral strike-slip faulting east of Xitieshan. Location shown in Figure 2. (e) Location of Figure 10a and local focal mechanisms as in Figure 4a.

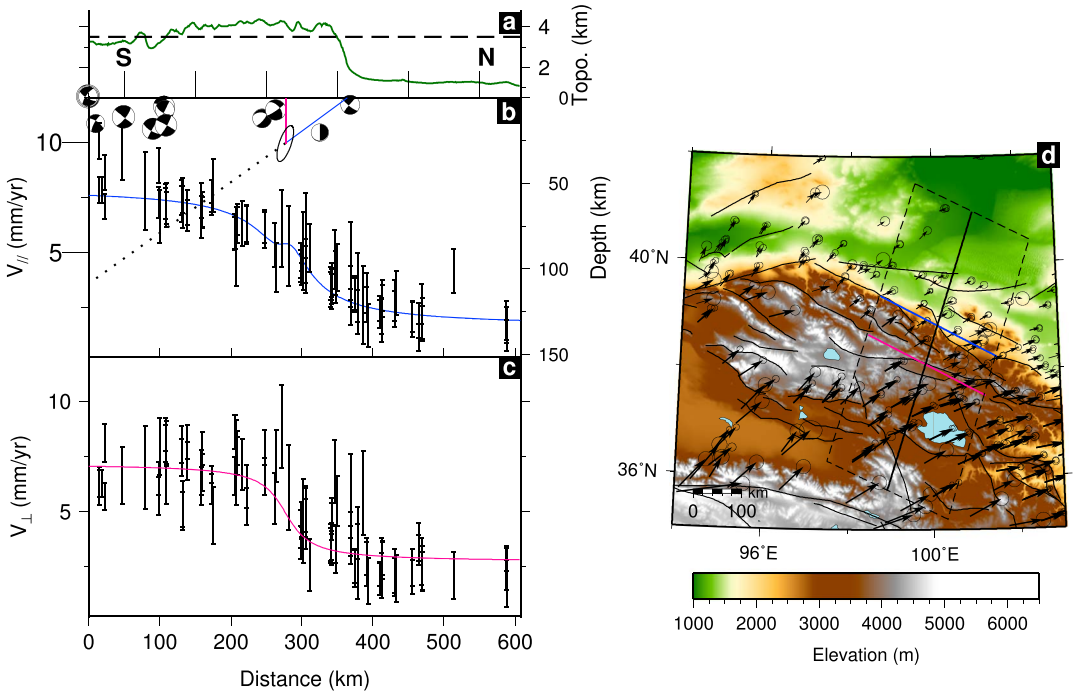


**Figure 11.** (a–d) One-fault elastic dislocation model for interseismic deformation in the Qilian Shan. Figure 11a shows topographic profile from dashed box within Figure 11d, from SRTM data. Figure 11b shows best fit model fault geometry, earthquake focal mechanisms, and fit to data for profile-parallel velocities. The dashed black straight line shows the geometry of the single creeping detachment fault with oblique slip, and the black ellipse shows the 95% uncertainty on the location of the locked-creeping transition. Above this pointth, the blue and pink solid lines show the inferred geometry of the locked thrust and strike-slip faults, onto which the oblique slip is inferred to be partitioned. Focal mechanisms show location of earthquakes from Figure 4a for the region of Figure 11d. The black vertical bars show GPS-derived velocity components parallel to the section line with 2-sigma uncertainties, and the blue line shows predicted velocities for the model geometry shown in the same panel. The black vertical bars show velocity components normal to the section line with 2-sigma uncertainties (Figure 11c), and the pink line shows predicted velocities for the model geometry shown in Figure 11b. Figure 1112d shows the map of GPS data from *Kreemer et al*. [2014] compilation. The dashed box shows region of GPS data projected onto central profile line for Figures 11b and 11c, and the pink and blue lines show surface projection of the strike-slip and thrust model faults.

*Yuan et al*. [2011] suggested that the northwestern end of the strike-slip Riyueshan Fault terminated in a thrust but did not examine the structure in this region. We confirm that a south dipping thrust places Proterozoic rocks over Jurassic coal measures at the end of the Riyueshan Fault (Figures 2 and 6h), but the topography is subdued, with no strong indications of Holocene activity.

In summary, left-lateral faulting within the Qilian Shan is focused on the Haiyuan Fault, as far west as its termination in the Sule Nanshan, but the fault zone is up to ~10 km wide and complex, and includes segments that both cross and lie parallel to the regional Paleozoic basement grain. Shorter right-lateral faults are also present within the Qilian Shan, additional to the Elashan and Riyueshan faults previously documented.

### 3.2. Constraints From Geodetic Data and Elastic Dislocation Modeling

GPS studies have previously established a horizontal velocity field for our area of interest [*Gan et al*., 2007; *Liang et al*., 2013] (Figure 11). In a Eurasian reference frame, interseismic velocities decrease from ~20 mm $yr^{-1}$ in the northern Kunlun to ~2–3 mm $yr^{-1}$ in the Alashan, on the edge of the Hexi Corridor, and exhibit partitioning of oblique convergence into components that are orthogonal and parallel to regional fault trends [*Zhang et al*., 2004; *Zheng et al*., 2013a]. Previous studies have used elastic dislocation models to interpret the GPS data but have mainly focused on modeling the range-parallel strike-slip component, thought to be largely accommodated on the left-lateral Haiyuan fault, and in contrast have suggested that the

**Table 1.** Elastic Dislocation Model Parameters for Initial Model With Two Separate Faults and for Final Model With One Fault and Oblique Slip at Depth[a]

| Model Fault Type | | Slip-Rate (mm $yr^{-1}$) | Locking Depth (km) | Dip (deg) | Location of Locked-Creeping Transition along Profile (km) | Offset in Velocity (mm $yr^{-1}$) | RMS (mm $yr^{-1}$) |
|---|---|---|---|---|---|---|---|
| Two faults | Dip slip | 6.0 ± 0.4 | 20[b] | 13 ± 2 S[c] | 49 ± 12[c] | 4.9 ± 0.2 | 0.78 |
| | Strike slip | 4.1 ± 0.8 | 18 ± 21 | 90[b] | 63 ± 6 | 4.3 ± 0.2 | 1.03 |
| One fault, two slip components | Dip slip | 6.7 ± 1.0 | 26 ± 8 | 17 ± 4 S | 49 ± 9 | 4.8 ± 0.2 | 0.74 |
| | Strike slip | 4.2 ± 0.4 | | | | 4.4 ± 0.2 | 1.06 |

[a]Uncertainties are at 2-sigma level.
[b]Fixed in inversion.
[c]When depth is fixed, dip, and location of fault covary.

convergent strain is broadly distributed across the Qilian Shan [*Zheng et al*., 2013a; *Zhang et al*., 2013]. In these models, the investigation of model fault locations and geometries is often precluded, as these details are fixed a priori.

Here we adopt a different approach to test whether the observed range-normal and range-parallel velocities across the Qilian Shan are consistent with interseismic strain accumulation across a single, localized detachment thrust and a subvertical strike-slip fault respectively. In this approach, the geometry and location of the faults are free parameters, which enable us to investigate if such a simple two fault model can fit the available data, and if it can, the geometry and location of these structures, along with the relationship between them. In particular, this is a quantitative test of existing models that propose the existence of an active regional detachment thrust below the entire Qilian Shan that accommodates the majority of the convergence across the mountain belt [*Meyer et al*., 1998; *Yin et al*., 2008b], as opposed to suggestions that convergence is broadly distributed across the mountain belt with little evidence of localization [*Zheng et al*., 2013a; *Zhang et al*., 2013].

#### 3.2.1. Two-Fault Model

First we draw a profile orientated N20°E, orthogonal to regional fault trends (Figure 11a), and project published GPS velocities onto the profile line from within ~250 km, separating the profile-parallel (shortening) and profile-perpendicular (strike-slip) velocities (Figures 11b and 11c). We have used published GPS data from the GEM Strain Rate Model compilation [*Liang et al*., 2013; *Kreemer et al*., 2014, and references therein] (Figure 11d). Initially, we model the horizontal velocity components separately with two model faults, in each case using a back slip calculation for a dislocation in an elastic half space, where the modeled fault is locked by friction above a "locking" depth and slips freely below this depth [*Savage and Burford*, 1973; *Savage*, 1983]. The model parameters for the strike-slip fault are slip rate, locking depth and location of the fault, as well as a static offset in velocity to account for anon zero reference. For the thrust fault, we fix the surface projection of the fault to the northern range front of the Qilian Shan and solve for slip rate, locking depth, and dip of the fault, along with a static offset in velocity to again account for a nonzero reference. The horizontal location of the locked-creeping transition is also a parameter of interest but is not independent; it is constrained solely by the dip and locking depth. For both models, we use a weighted nonlinear least squares inversion with multiple restarts to avoid local minima. We estimate uncertainties on each model using a Monte Carlo approach, perturbing the GPS data 100 times with noise based on the formal velocity uncertainties and inverting these perturbed data sets using the same process detailed above. The spread of the 100 retrieved values for each model parameter defines the uncertainty on that parameter. More details of the code used are available from the authors on request.

We make one additional modification to our two-fault model: the best fit detachment fault has a locking depth of 35 ± 15 km (2-sigma), which is much greater than the estimated 20 km seismogenic thickness [*Sloan et al*., 2011] and would lie within the lower crust for this region. We therefore fix the depth to 20 km, with very little degradation to the fit to the data (see Figures S1 and S2 and Table S3 in the supporting information).

Our two-fault model is presented in Table 1 and Figure S1 and fits the GPS data well, with residuals of similar magnitude to the formal uncertainty on the data (~1 mm/yr). The most important results of this model are the following: (1) that the range-normal component of the GPS data can be explained by slip on a localized detachment at depth and (2) that the data strongly constrain the location of the locked-creeping transition of the detachment to be coincident (within uncertainty) with the locked-creeping transition for the strike-slip fault and with the mapped trace of the Haiyuan fault. Essentially,

the locked portion of the strike-slip fault lies above the locked-creeping transition of the detachment thrust (Figures 3 and S1b). We note that the dip angle and dip direction of the detachment thrust are not well constrained, but although models with different dip values provide similar fit to the data (Figures S2 and S3), the observation of the intersection at depth of the strike-slip and detachment thrust is robust irrespective of dip direction, for locking depths $<$20 km. Here we present the south dipping solution as this seems more realistic, given the location of the Qilian Shan at the northeastern side of the Tibetan Plateau. In the *Savage and Burford* [1973] elastic model for strike-slip faulting used here, fault-parallel surface velocities do not depend at all on the dip of the strike-slip fault below the locking-depth. Therefore, the simplest interpretation of the coincidence between the locked-creeping transitions of the two model faults is that the dip of the strike-slip fault at depth is the same as the detachment, i.e., that oblique slip is localized on a single dipping detachment at depth, and is partitioned only in the seismogenic crust.

#### 3.2.2. One-Fault Model

We test this interpretation formally by running one final inversion. We use the same method described above but this time constrain both strike-slip and thrust components of slip to take place on a single dipping detachment below one locking depth, simultaneously fitting both profile-perpendicular and profile-parallel GPS velocities. The joint inversion of both components of velocity means that the locking depth is better constrained than in the previous inversions, so it is not fixed in this model. When compared to the two-fault model, the resulting one-fault oblique-slip model fits the data with no significant degradation to misfit and is presented in Table 1 and Figure 11.

The best fit oblique detachment slips below a locking depth of 26 ± 8 km and has a dip of 17 ± 4° to the SSW. This locking depth is in close agreement with estimates of the seismogenic thickness from robust earthquake depths (~20 km [*Sloan et al*., 2011]) and with previous interseismic studies of the Haiyuan fault west of 104°E [*Jolivet et al*., 2012], which is fully locked, in contrast to the creeping section further east [e.g., *Jolivet et al*., 2015; *Daout et al*., 2016]. The best fit horizontal location of the locked-creeping transition on the fault is constrained to within 9 km and is in agreement with the mapped surface trace of the Haiyuan Fault, implying a vertical or subvertical structure in the seismogenic upper crust. The rate of strike-slip motion on the detachment is 4.2 ± 0.4 mm $yr^{-1}$, consistent with previous estimates for the slip-rate on the Haiyuan fault in this region [e.g., *Zhang et al*., 2004; *Cavalie et al*., 2008; *Jolivet et al*., 2012; *Zheng et al*., 2013a]. The rate of reverse dip-slip motion on the detachment is 6.7 ± 1.0 mm $yr^{-1}$. It is important to note that although we draw the shallow, locked thrust fault that accommodates this strain in the seismogenic crust as a low-angle continuation of the detachment (Figure 3), which matches geologic data (Figure 5) [*Zuza et al*., 2016], this is not a requirement of the dislocation model itself. The model does not predict the structure within the locked region of the crust, i.e., whether the dislocation continues updip at a low angle or into one or more steeper structures. From the ratio of strike-slip and dip-slip rates (Table 1), we estimate the rake on the detachment at depth to be ~58°.

The geometric relation proposed here between major strike-slip and thrust faults has been inferred from geodetic data above subduction zones with oblique convergence and is suggested from numerical models to result from localization of shear strain in the crust above the locked-creeping transition on the detachment [*McCaffrey et al*., 2000]. This relationship has not been previously identified for the Qilian Shan (although it was predicted by the models of *Bowman et al*. [2003]) and is highly likely to occur in other continental fold-and-thrust belts where strain partitioning has also been recognized [e.g., *Murphy et al*., 2014; *Silver et al*., 2015].

### 3.3. Regional Scale Geomorphology and Drainage Patterns

We have examined regional patterns of topography and drainage to add at least first-order insights to our fieldwork, remote sensing, and dislocation models. Smoothed elevation values (Figure 4a) and slope values (Figure 12) highlight that the highest elevation and lowest relief part of the Qilian Shan occurs in the middle of the region, centered on Hala Lake. Regional elevations decrease away from this area in all directions, including toward the Altyn Tagh Fault to the west and north.

Rivers in the east of the Qilian Shan that do not drain into the Yellow River typically flow into Hala or Qinghai lakes (Figure 2). Rivers in the west flow to the WNW along the major valleys parallel to the range fronts

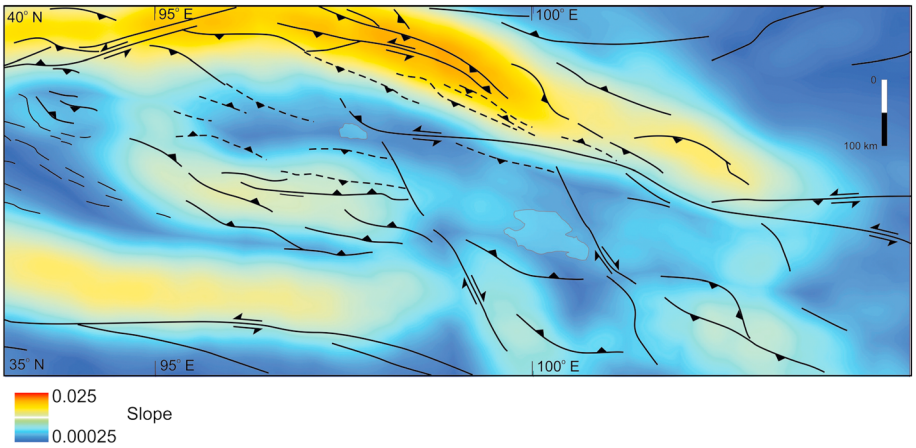


**Figure 12.** Regional slope, derived from a 35 km radius moving window on mean elevation smoothed over a 75 km radius moving window.

(Figure 13), but three of the major ones are diverted northward before they reach the Altyn Tagh Fault. This northward diversion produce a nested pattern to the drainage (Figure 13), with the southernmost river, the Sule He, reaching furthest west, while rivers to the east, the Beida He and Hong Shuiba He, have the shorter courses and more easterly diversion points.

## 4. Discussion

### 4.1. Finite Strain Estimates

Throw estimates of ~5 km for individual range fronts within the Qilian Shan can be summarized to estimate the overall range-normal shortening (Figure 5). We use an estimate of thrust dip of 45°, based on focal mechanism fault dips (Figure 4b) and the dips of exposed range-bounding thrusts (Figure 7). Thrusts are assumed to be planar, at least at the upper crustal levels under consideration. The throw corresponds to a horizontal shortening (heave) of ~5 km. Given the seven main internal range fronts in our longer section, this configuration suggests roughly 35 km of Cenozoic shortening across the section or ~30%. Extrapolating across the full width of the Qilian Shan ranges (presently ~250–300 km, increasing westward) gives ~110–130 km of thrust-related shortening in the Cenozoic within the interior of the Qilian Shan. An estimated 10–15% shortening is expressed in the folded strata of the intermontane basins (section 3.1.1), equivalent to a further ~15 km shortening across the whole range.

The above estimate does not include the northern margin of the Qilian Shan, which differs from the internal range fronts in size of the topographic step down to the Hexi Corridor basins to the north (Figures 4a and 13) and the lower fault dip. A recent interpretation of seismic reflection profiles across this northern margin

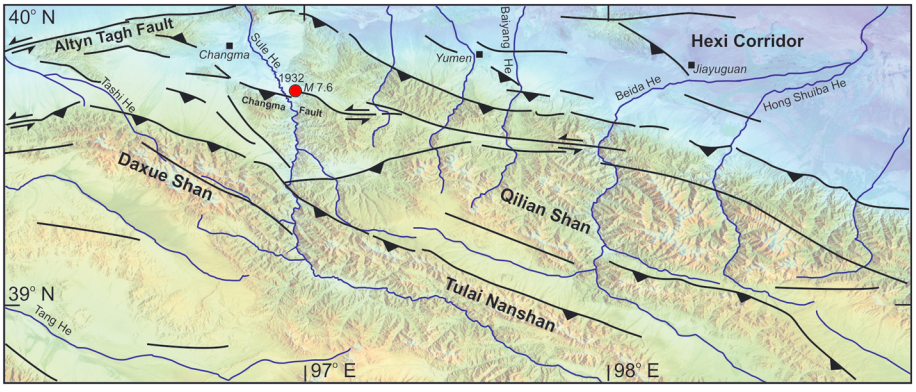


**Figure 13.** Drainage patterns and late Cenozoic faults in the northwest Qilian Shan. Background is SRTM digital topography superimposed over Landsat 7 false color imagery (bands 7, 4, and 2).

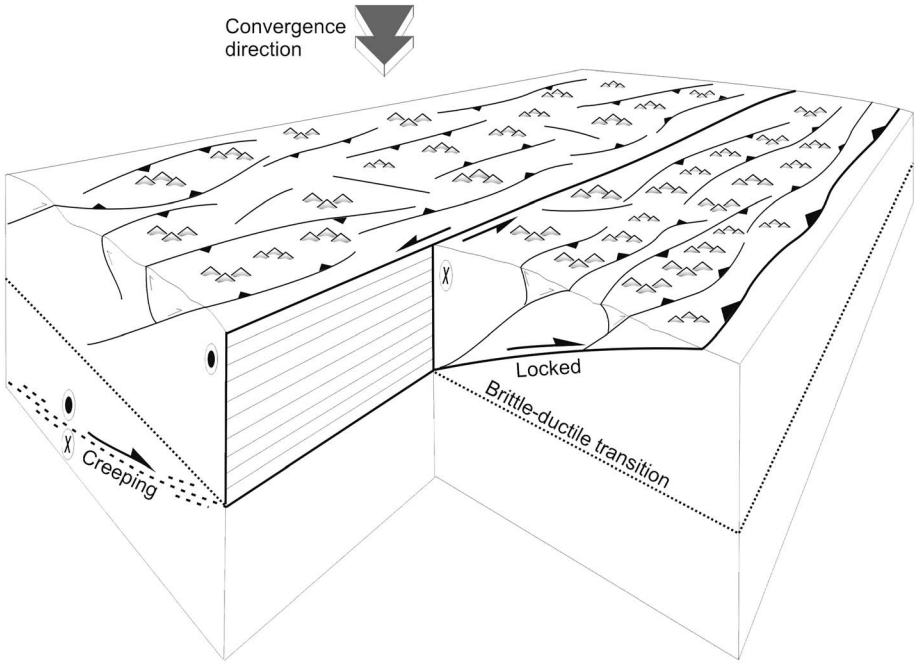


**Figure 14.** Schematic illustration of the fault geometry proposed for the Qilian Shan, with partitioning of oblique convergence onto strike-slip and thrust components, with the intersection of the strike-slip and thrust faulting taking place at the down-dip limit of the locked portion of the thrust.

suggests typically ~30 km of shortening on this thrust front alone [*Zuza et al*., 2016], on a thrust system dipping south at ~15°, which is consistent with the 17° dip for the shear zone underlying the range derived from the elastic dislocation model in this study (Figure 11). Adding this 30 km value to the shortening estimate for the internal ranges gives a total of 155–175 km range-normal shortening across the Qilian Shan. Previous interpretations of the amount of shortening at the northern, marginal, range front are lower than 30 km, at ≤10 km [*Zheng et al*., 2010]. If this lower figure is correct, the overall shortening estimate must be reduced accordingly.

It has been previously suggested that at ~15 Ma there was the onset or acceleration of significant deformation and uplift in the northeastern part of the Tibetan Plateau, including the Qilian Shan [e.g., *Duvall et al*., 2013]. *Zheng et al*. [2010] put the onset of significant late Cenozoic exhumation near the northern thrust in Qilian Shan to be slightly later, at 10 Ma, based on (U-Th)/He thermochronometry. Current GPS-derived deformation rates for convergence across the Qilian Shan are 7.7 mm $yr^{-1}$, combining dip-slip and strike-slip components (section 3.2.2). Extrapolating this rate to 15 Ma would mean ~115 km of total shortening across the Qilian Shan and Qaidam Basin, roughly split into ~65 km of strike-slip offset on the Haiyuan Fault, and ~100 km of range-normal shortening. The extrapolated range-normal shortening estimate is comparable to, if lower than, our estimate in this study of 155–175 km and the estimate of 150–200 km shortening of *Meyer et al*. [1998]. It is distinctly lower than the >215 km derived by *Zuza et al*. [2016] and the 250 km proposed by *Cheng et al*. [2015]. The differences relate to the amount of strain interpreted for the internal ranges, which should clearly be a focus for future study. If the higher estimates of *Zuza et al*. [2016] and *Cheng et al*. [2015] are more realistic, strain needs to have taken place at near present rates for much longer than 15 Myr or episodically through the Cenozoic. Our 155–175 km estimate fits a scenario where the present shortening rate has occurred since ~15 Ma, and achieved most of the finite strain, but leaves open the possibility for significant strain before 15 Ma.

### 4.2. Crustal Scale Accommodation of Oblique Convergence

Elastic dislocation modeling (Figure 11) provides an approach for understanding the deep structure of the region. The best fit model for the interseismic geodetic data is consistent with localized, oblique, aseismic slip on a low-angle detachment thrust (17° dip) below a locking depth fixed of 26 km (Figure 14). A significant

result of this model is that the locked-creeping transition lies directly beneath the location of the strike-slip Haiyuan Fault. This implies that strain is spatially partitioned in the seimogenic upper crust between strike-slip motion on the vertical Haiyuan Fault and thrusting, possibly to a large extent on the updip continuation of the detachment (Figure 11). This deformation pattern is similar to geodetic observations made across oblique oceanic subduction zones [*McCaffrey et al*., 2000] and suggests that such behavior also occurs during strain partitioning in continental fold-and-thrust belts. It matches the model predictions of *Bowman et al*. [2003]. A similar, but not identical, pattern of strain partitioning has been interpreted for the Haiyuan Fault and adjacent thrusts, to the east of our study area (102–104°E), by *Daout et al*. [2016], based on a combined study of InSAR and GPS data. The two areas are different in terms of the proportions of thrust and strike-slip deformation and the greater depth of locking further west. A more fundamental difference is that *Daout et al*. [2016] do not model the seismogenic strike-slip fault as directly above locked-creeping transition, as is found in our paper.

The historical events of $M \sim 7$ (Figure 4a) may be a record of rare but large earthquakes related to such a detachment, above the locking depth. It is not clear from the structures exposed within the Qilian Shan or our analysis of the geodetic data that the deep structure corresponds to a crustal scale critical wedge [*Meyer et al*., 1998] or a continental subduction zone [*Guillot and Replumaz*, 2013]. The regional topography (Figures 4a, 11, and 12) shows steep margins on both the northern and southern sides of the range, with lower internal slopes, not consistent with a crustal wedge thickening southward toward the main part of the Tibetan Plateau.

It is notable that there is a clear instrumental seismicity record of relatively steep thrusts (≥30°; Figure 4a), but no focal mechanisms that clearly correspond to seismic slip on the underlying detachment thrust. It could be that seismic slip on these steeper thrusts reduces the overall slip deficit on the detachment thrust and reduces the magnitude of an eventual earthquake on the detachment.

We speculate that the detachment thrust corresponds to the upper surface of the North China Block (Figure 3), proposed by some authors [e.g., *Yin et al*., 2008b] to underlie most or all of the Qilian Shan, and consistent with deep seismic evidence [*Ye et al*., 2015]. Given the lack of hundred kilometer-scale Cenozoic thrusting at the northern margin of the Qilian Shan [*Hetzel et al*., 2004; *Zheng et al*., 2010; *Zuza et al*., 2016; this study], we conclude that the main underthrusting of the North China Block (Figure 3) is more likely to have taken place during the Paleozoic accretion of the Qilian Shan, with reactivation during late Cenozoic deformation. There is evidence for this Paleozoic age for underthrusting, in the zircon populations within Paleozoic plutons in the Qilian Shan, which contain Precambrian signatures of the North China Block [*Gehrels et al*., 2003].

The structure of the Qilian Shan has similarities to the Himalayas, where the Indian Plate underthrusts Eurasian crust along a major thrust, dipping at a similar angle [e.g., *Murphy et al*., 2014]. There is no evidence that the underthrust North China Block underwent slab break-off and uplift in the Cenozoic, comparable to the India-Eurasia system [*Magni et al*., 2017].

### 4.3. Thrust Distribution, Crustal Thickening, and Surface Uplift

There is a concentration of $M > 5$ thrust events at or below the regional 3500 m elevation contour (Figure 4a). Of the few $M > 5$ thrust events that occurred at higher elevations, one occurs on a restraining bend along the Haiyuan Fault and two are ~100 km from the Altyn Tagh Fault. $M > 4$ events occur at higher elevations (Figure 4a) but mainly on the northern side of the range. The area west of Lake Hala is distinctly aseismic. While no focal mechanisms are available for these smaller events, it seems reasonable to conclude that they are mainly thrust earthquakes in keeping with the observed structure of the region. Events along the Haiyuan Fault are more likely to be strike slip. The higher, interior regions of the Qilian Shan show less evidence of Holocene thrust activity than lower elevation regions (Figure 4a). The interior of the Qilian Shan has more subdued relief than the range margins [*Liu-Zeng et al*., 2008] (Figure 12). The combined low relief and low seismicity give the interior region plateau-like characteristics, at least in incipient form.

### 4.4. Influence of the Altyn Tagh Fault

It has been previously proposed that thrusts in the Qilian Shan splay off the northeastern part of the Altyn Tagh Fault, for up to ~400 km away from the latter, and owe their existence to the need to absorb the slip along this structure. [*Meyer et al*., 1998; *Van der Woerd et al*., 2001; *Cheng et al*., 2015]. There is clearly

interaction between the thrusts in the Qilian Shan and the Altyn Tagh Fault: the thrusts in the northwest of the Qilian Shan change strike westward, to swing into alignment (Figure 2). Active thrusting occurs relatively close to the fault, at high regional elevations, in contrast to the remainder of the Qilian Shan further east (Figure 4a).

However, the regional elevations of the Qilian Shan decrease toward the Altyn Tagh Fault (Figures 4a and 12), implying that the greatest crustal thickening and highest topography has developed in the interior of the Qilian Shan, rather than dying away laterally from the Altyn Tagh Fault. The pattern of rivers in the northwestern Qilian Shan is consistent with an origin whereby drainage flows westward away from the interior of the range, before meeting uplifted areas influenced by the Altyn Tagh Fault, and being diverted northward toward the Hexi Corridor (Figure 13). Therefore, the influence of the Altyn Tagh Fault may extend laterally only 100–200 km into the interior of the Qilian Shan, with most of the thrusting along the range representing a regional shortening as part of the India-Eurasia convergence. There is clearly a lot of scope for more work on this subject, but our observations in Figures 12 and 13 are consistent with the other results in this paper, whereby the thrusting in the Qilian Shan is a major part of the overall India-Eurasia convergence and not a secondary feature arising from the slip along the Altyn Tagh Fault.

We also note the coincidence of Cenozoic thrusts with Paleozoic structural boundaries along the length of the Qilian Shan [*Song et al*., 2013; *Wu et al*., 2016], i.e., for ~800 km, and strongly implicating reactivation of basement faults as a factor in controlling the location of the young structures (Figure 2). Our fieldwork observations confirm this match, with the exception of the Xitieshan region (Figure 7), where the Paleozoic foliations strike more north-south than the Cenozoic thrusts in the same region.

## 5. Conclusions

We estimate range-normal shortening across the Qilian Shan as ~155–175 km, comparable to the 150–200 km claimed from crustal scale restorations by *Meyer et al*., 1998], but lower than the >215 km and 250 km values derived by *Zuza et al*. [2016] and *Cheng et al*. [2015]. Maintaining the present range-normal shortening rate of 6.4 mm $yr^{-1}$ for the 15 Myr since the inferred onset or acceleration of deformation in the Qilian Shan yields ~100 km total range-normal shortening, which is to a first order consistent with our estimate, but raises the possibility that some strain took place before 15 Ma or has even slowed since 15 Ma.

The overall structure of the Qilian Shan is divergent, with southward thrusting at the southern margin and northward thrusting at the northern margin of the range. Thrust structure within the region shows no predominant transport direction at upper crustal levels (Figure 5).

Elastic dislocation modeling indicates that a single regional detachment thrust (dip angle of 17°) with oblique slip below 26 km depth can explain both range-parallel and range-normal components of the GPS-derived interseismic velocity field (Figure 11). Upper and lower crustal deformation therefore appear to be decoupled along a zone approximating simple shear under the Qilian Shan (Figure 14).

This shear zone may be the upper surface of an underthrust North China Block [*Yin et al*., 2008b] (Figure 3), with the caveat that regional underthrusting is more likely to have taken place in the Paleozoic than the Cenozoic. The dip angle is higher than commonly proposed critical wedge scenarios for individual fold-and-thrust belts, which have much lower dip values for the basal detachment to the fold-and-thrust belt [*Davis et al*., 1983].

The strike-slip component of deformation is located on a near-vertical structure above the updip limit of oblique interseismic slip on the model detachment and equivalent to the observed Haiyuan Fault. This configuration of strain partitioning may apply more generally in zones of oblique convergence (Figure 14) and so explain the location of strike-slip faults in other fold-and-thrust belts, both ancient and active [e.g., *Holdsworth and Strachan*, 1991].

Well-constrained thrust focal mechanisms dip typically at >30° (Figure 4b) and are confined to the upper 20 km of the crust [*Sloan et al*., 2011]. If the crustal-scale structure involves an underlying low-angle thrust (Figures 3 and 11), it has not produced earthquakes recorded in the instrumental catalogs. However, historic $M \sim 7$ events at the northern side of the Qilian Shan could correspond to seismic slip on this structure (Figure 4a).

Major thrust seismicity ($M > 5$) in the Qilian Shan diminishes above the regional 3500 m contour, and the few large thrust events above this elevation are typically linked to strike-slip faults at restraining bends (Figure 4a). Smaller earthquakes are more widespread across the Qilian Shan (Figure 4a). Combined with the subdued relief at these higher elevations (Figure 12), it appears that the interior of the Qilian Shan is developing plateau-like characteristics.

The influence of the Altyn Tagh Fault may be confined to adjacent parts of the Qilian Shan, within 100–200 km, and not the full lateral extent of thrusted ranges. These Cenozoic thrusts follow the Paleozoic basement grain for ~800 km to the ESE, along the Qilian Shan [*Song et al*., 2013; *Wu et al*., 2016], and strongly imply that reactivation of Paleozoic structures controls the location of the modern faults.

**Acknowledgments**
Data supporting Figure 4 are available in Tables S1 and S2. SRTM digital topography is from http://www2.jpl.nasa.gov/srtm/. This work was supported by the Natural Environment Research Council (grant NE/H021620/1) and the National Natural Science Foundation of China (grants 41372060 and 41121062). Fieldwork was supported by Chinese Geological Survey grants (1212011121092 and 1212011220928) to Yaoling Niu and a Durham University travel grant to M.B.A. Thanks to Romain Jolivet and Richard Styron for their constructive reviews.

## References

Avouac, J. P., and P. Tapponnier (1993), Kinematic model of active deformation in central Asia, *Geophys. Res. Lett.*, *20*, 895–898, doi:10.1029/93GL00128.

Bowman, D., G. King, and P. Tapponnier (2003), Slip partitioning by elastoplastic propagation of oblique slip at depth, *Science*, *300*, 1121–1123.

Burchfiel, B. C., Q. D. Deng, P. Molnar, L. Royden, Y. P. Wang, P. Z. Zhang, and W. Q. Wang (1989), Intracrustal detachment within zones of continental deformation, *Geology*, *17*, 748–752.

Burchfiel, B. C., P. Z. Zhang, Y. P. Wang, W. Q. Zhang, F. M. Song, Q. D. Deng, P. Molnar, and L. Royden (1991), Geology of the Haiyuan Fault Zone, Ningxia-hui Autonomous Region, China, and its relation to the evolution of the northeastern margin of the Tibetan Plateau, *Tectonics*, *10*, 1091–1110, doi:10.1029/90TC02685.

Cavalie, O., C. Lasserre, M. P. Doin, G. Peltzer, J. Sun, X. Xu, and Z. K. Shen (2008), Measurement of interseismic strain across the Haiyuan fault (Gansu, China), by InSAR, *Earth Planet. Sci. Lett.*, *275*, 246–257.

Champagnac, J.-D., D.-Y. Yuan, W.-P. Ge, P. Molnar, and W.-J. Zheng (2010), Slip rate at the north-eastern front of the Qilian Shan, China, *Terra Nova*, *22*, 180–187.

Chen, G. H., X. W. Xu, A. L. Zhu, X. Q. Zhang, R. M. Yuan, Y. Klinger, and J. M. Nocquet (2013), Seismotectonics of the 2008 and 2009 Qaidam earthquakes and its implication for regional tectonics, *Acta Geol. Sin. English Edition*, *87*, 618–628.

Chen, W. P., C. Y. Chen, and J. L. Nabelek (1999), Present-day deformation of the Qaidam basin with implications for intra-continental tectonics, *Tectonophysics*, *305*, 165–181.

Cheng, F., M. Jolivet, G. Dupont-Nivet, L. Wang, X. J. Yu, and Z. J. Guo (2015), Lateral extrusion along the Altyn Tagh Fault, Qilian Shan (NE Tibet): Insight from a 3D crustal budget, *Terra Nova*, *27*, 416–425.

Clark, M. K., K. A. Farley, D. Zheng, Z. Wang, and A. R. Duvall (2010), Early Cenozoic faulting of the northern Tibetan Plateau margin from apatite (U-Th)/He ages, *Earth Planet. Sci. Lett.*, *296*, 78–88.

Cowgill, E., R. D. Gold, X. H. Chen, X. F. Wang, J. R. Arrowsmith, and J. Southon (2009), Low Quaternary slip rate reconciles geodetic and geologic rates along the Altyn Tagh fault, northwestern Tibet, *Geology*, *37*, 647–650.

Daout, S., R. Jolivet, C. Lasserre, M. P. Doin, S. Barbot, P. Tapponnier, G. Peltzer, A. Socquet, and J. Sun (2016), Along-strike variations of the partitioning of convergence across the Haiyuan fault system detected by InSAR, *Geophys. J. Int.*, *205*, 536–547.

Davis, D., J. Suppe, and F. A. Dahlen (1983), Mechanics of fold-and-thrust belts and accretionary wedges, *J. Geophys. Res.*, *88*, 1153–1172, doi:10.1029/JB088iB02p01153.

Ding, G. Y., J. Chen, Q. J. Tian, X. H. Shen, C. Q. Xing, and K. B. Wei (2004), Active faults and magnitudes of left-lateral displacement along the northern margin of the Tibetan Plateau, *Tectonophysics*, *380*, 243–260.

Duvall, A. R., and M. K. Clark (2010), Dissipation of fast strike-slip faulting within and beyond northeastern Tibet, *Geology*, *38*, 223–226.

Duvall, A. R., M. K. Clark, E. Kirby, K. A. Farley, W. H. Craddock, C. Y. Li, and D. Y. Yuan (2013), Low-temperature thermochronometry along the Kunlun and Haiyuan Faults, NE Tibetan Plateau: Evidence for kinematic change during late-stage orogenesis, *Tectonics*, *32*, 1190–1211, doi:10.1002/tect.20072.

Elliott, J. R., R. J. Walters, P. C. England, J. A. Jackson, Z. Li, and B. Parsons (2010), Extension on the Tibetan Plateau: Recent normal faulting measured by InSAR and body wave seismology, *Geophys. J. Int.*, *183*, 503–535.

Elliott, J. R., B. Parsons, J. A. Jackson, X. Shan, R. A. Sloan, and R. T. Walker (2011), Depth segmentation of the seismogenic continental crust: The 2008 and 2009 Qaidam earthquakes, *Geophys. Res. Lett.*, *38*, L06305, doi:10.1029/2011GL046897.

England, P., and P. Molnar (2005), Late Quaternary to decadal velocity fields in Asia, *J. Geophys. Res.*, *110*, B12401, doi:10.1029/2004JB003541.

Feng, M., P. Kumar, J. Mechie, W. Zhao, R. Kind, H. Su, G. Xue, D. Shi, and H. Qian (2014), Structure of the crust and mantle down to 700 km depth beneath the East Qaidam basin and Qilian Shan from P and S receiver functions, *Geophys. J. Int.*, *199*, 1416–1429.

Gan, W. J., P. Z. Zhang, Z. K. Shen, Z. J. Niu, M. Wang, Y. G. Wan, D. M. Zhou, and J. Cheng (2007), Present-day crustal motion within the Tibetan Plateau inferred from GPS measurements, *J. Geophys. Res.*, *112*, B08416, doi:10.1029/2005JB004120.

Gaudemer, Y., P. Tapponnier, B. Meyer, G. Peltzer, S. M. Guo, Z. T. Chen, H. G. Dai, and I. Cifuentes (1995), Partitioning of crustal slip between linked, active faults in the eastern Qilian Shan, and evidence for a major seismic gap, the Tianzhu Gap, on the western Haiyuan Fault, Gansu (China), *Geophys. J. Int.*, *120*, 599–645.

Gehrels, G. E., A. Yin, and X. F. Wang (2003), Magmatic history of the northeastern Tibetan Plateau, *J. Geophys. Res.*, *108*(B9), 2423, doi:10.1029/2002JB001876.

Geological Bureau of Qinghai Province (1968a), Qilian, Geological Bureau Qinghai Province.

Geological Bureau of Qinghai Province (1968b), Yeniutai, Geological Bureau Qinghai Province.

Geological Bureau of Qinghai Province (1980), Huaitucun, Geological Bureau Qinghai Province.

Guillot, S., and A. Replumaz (2013), Importance of continental subductions for the growth of the Tibetan Plateau, *Bull. Soc. Geol. Fr.*, *184*, 199–223.

Hetzel, R., M. X. Tao, S. Stokes, S. Niedermann, S. Ivy-Ochs, B. Gao, M. R. Strecker, and P. W. Kubik (2004), Late Pleistocene/Holocene slip rate of the Zhangye thrust (Qilian Shan, China) and implications for the active growth of the northeastern Tibetan Plateau, *Tectonics*, *23*, TC6006, doi:10.1029/2004TC001653.

Holdsworth, R. E., and R. A. Strachan (1991), Interlinked system of ductile strike-slip and thrusting formed by Caledonian sinistral transpression in northeastern Greenland, *Geology*, *19*, 510–513.

Horton, B. K., G. Dupont-Nivet, J. Zhou, G. L. Waanders, R. F. Butler, and J. Wang (2004), Mesozoic-Cenozoic evolution of the Xining-Minhe and Dangchang basins, northeastern Tibetan Plateau: Magnetostratigraphic and biostratigraphic results, *J. Geophys. Res.*, *109*, B04402, doi:10.1029/2003JB002913.

Jolivet, R., C. Lasserre, M. P. Doin, S. Guillaso, G. Peltzer, R. Dailu, J. Sun, Z. K. Shen, and X. Xu (2012), Shallow creep on the Haiyuan Fault (Gansu, China) revealed by SAR interferometry, *J. Geophys. Res.*, *117*, B06401, doi:10.1029/2011JB008732.

Jolivet, R., T. Candela, C. Lasserre, F. Renard, Y. Klinger, and M. P. Doin (2015), The burst-like behavior of aseismic slip on a rough fault: The creeping section of the Haiyuan Fault, China, *Bull. Seismol. Soc. Am.*, *105*(1), 480–488.

Kreemer, C., G. Blewitt, and E. C. Klein (2014), A geodetic plate motion and global strain rate model, *Geochem., Geophys., Geosyst.*, *15*, 3849–3889, doi:10.1002/2014GC005407.

Lease, R. O., D. W. Burbank, M. K. Clark, K. A. Farley, D. W. Zheng, and H. P. Zhang (2011), Middle Miocene reorganization of deformation along the northeastern Tibetan Plateau, *Geology*, *39*, 359–362.

Lee, W. H. K., F. T. Wu, and C. Jacobsen (1976), Catalog of historical earthquakes in China compiled from recent Chinese publications, *Bull. Seismol. Soc. Am.*, *66*, 2003–2016.

Liang, S. M., W. J. Gan, C. Z. Shen, G. R. Xiao, J. Liu, W. T. Chen, X. G. Ding, and D. M. Zhou (2013), Three-dimensional velocity field of present-day crustal motion of the Tibetan Plateau derived from GPS measurements, *J. Geophys. Res. Solid Earth*, *118*, 5722–5732, doi:10.1002/2013JB010503.

Liu, R. C., M. B. Allen, Q. Q. Zhang, W. Du, X. Cheng, R. E. Holdsworth, and Z. J. Guo (2017), Basement controls on deformation during oblique convergence: Transpressive structures in the western Qaidam Basin, northern Tibetan Plateau, *Lithosphere*, doi:10.1130/L634.1.

Liu-Zeng, J., P. Tapponnier, Y. Gaudemer, and L. Ding (2008), Quantifying landscape differences across the Tibetan Plateau: Implications for topographic relief evolution, *J. Geophys. Res.*, *113*, F04018, doi:10.1029/2007JF000897.

Lu, S. N. (2002), *Preliminary Study of Precambrian Geology in the North Tibet–Qinghai Plateau*, Geological Publishing House, Beijing.

McCaffrey, R., P. C. Zwick, Y. Bock, L. Prawirodirdjo, J. F. Genrich, C. W. Stevens, S. S. O. Puntodewo, and C. Subarya (2000), Strain partitioning during oblique plate convergence in northern Sumatra: Geodetic and seismologic constraints and numerical modeling, *J. Geophys. Res.*, *105*, 28,363–28,376, doi:10.1029/1999JB900362.

Magni, V., M. B. Allen, J. van Hunen, and P. Bouilhol (2017), Continental underplating after slab break-off, *Earth Planet. Sci. Lett.*, *474*, 59–67.

Meyer, B., P. Tapponnier, L. Bourjot, F. Metivier, Y. Gaudemer, G. Peltzer, G. Shunmin, and C. Zhitai (1998), Crustal thickening in Gansu-Qinghai, lithospheric mantle subduction, and oblique, strike-slip controlled growth of the Tibet plateau, *Geophys. J. Int.*, *135*, 1–47.

Molnar, P., and H. Lyon-caen (1989), Fault plane solutions of earthquakes and active tectonics of the Tibetan Plateau and its margins, *Geophys. J. Int.*, *99*, 123–153.

Murphy, M. A., M. H. Taylor, J. Gosse, C. R. P. Silver, D. M. Whipp, and C. Beaumont (2014), Limit of strain partitioning in the Himalaya marked by large earthquakes in western Nepal, *Nat. Geosci.*, *7*, 38–42.

Palumbo, L., R. Hetzel, M. X. Tao, X. B. Li, and J. M. Guo (2009), Deciphering the rate of mountain growth during topographic pre-steady state: An example from the NE margin of the Tibetan Plateau, *Tectonics*, *28*, TC4017, doi:10.1029/2009TC002455.

Peltzer, G., P. Tapponnier, Y. Gaudemer, B. Meyer, S. M. Guo, K. L. Yin, Z. T. Chen, and H. G. Dai (1988), Offsets of late Quaternary morphology, rate of slip, and recurrence of large earthquakes on the Chang Ma Fault (Gansu, China), *J. Geophys. Res.*, *93*, 7793–7812, doi:10.1029/JB093iB07p07793.

Royden, L. H., B. C. Burchfiel, and R. D. van der Hilst (2008), The geological evolution of the Tibetan Plateau, *Science*, *321*, 1054–1058.

Savage, J. C. (1983), A dislocation model of strain accumulation and release at a subduction zone, *J. Geophys. Res.*, *88*, 4984–4996, doi:10.1029/JB088iB06p04984.

Savage, J. C., and R. O. Burford (1973), Geodetic determination of relative plate motion in central California, *J. Geophys. Res.*, *78*, 832–845, doi:10.1029/JB078i005p00832.

Şengör, A. M. C., and A. H. Okurogullari (1991), The role of accretionary wedges in the growth of continents: Asiatic examples from Argand to Plate Tectonicsl, *Eclogae Geo. Helv.*, *84*, 535–597.

Silver, C. R. P., M. A. Murphy, M. H. Taylor, J. Gosse, and T. Baltz (2015), Neotectonics of the western Nepal fault system: Implications for Himalayan strain partitioning, *Tectonics*, *34*, 2494–2513, doi:10.1002/2014TC003730.

Sloan, R. A., J. A. Jackson, D. McKenzie, and K. Priestley (2011), Earthquake depth distributions in central Asia, and their relations with lithosphere thickness, shortening and extension, *Geophys. J. Int.*, *185*, 1–29.

Song, S., Y. Niu, L. Su, and X. Xia (2013), Tectonics of the North Qilian orogen, NW China, *Gondwana Res.*, *23*, 1378–1401.

Song, S., Y. Niu, L. Su, C. Zhang, and L. Zhang (2014), Continental orogenesis from ocean subduction, continent collision/subduction, to orogen collapse, and orogen recycling: The example of the North Qaidam UHPM belt, NW China, *Earth Sci. Rev.*, *129*, 59–84.

Tapponnier, P., and P. Molnar (1977), Active faulting and tectonics in China, *J. Geophys. Res.*, *82*, 2905–2930, doi:10.1029/JB082i020p02905.

Tapponnier, P., et al. (1990), Active folding and thrusting in the Qilian Shan, and decoupling between upper crust and mantle in northeastern Tibet, *Earth Planet. Sci. Lett.*, *97*, 382–403.

Tapponnier, P., Z. Q. Xu, F. Roger, B. Meyer, N. Arnaud, G. Wittlinger, and J. S. Yang (2001), Oblique stepwise rise and growth of the Tibet plateau, *Science*, *294*, 1671–1677.

Taylor, M., and A. Yin (2009), Active structures of the Himalayan-Tibetan orogen and their relationships to earthquake distribution, contemporary strain field, and Cenozoic volcanism, *Geosphere*, *5*, 199–214.

Thatcher, W. (2007), Microplate model for the present-day deformation of Tibet, *J. Geophys. Res.*, *112*, B01401, doi:10.1029/2005JB004244.

Tian, X. B., and Z. J. Zhang (2013), Bulk crustal properties in NE Tibet and their implications for deformation model, *Gondwana Res.*, *24*, 548–559.

Van der Woerd, J., X. W. Xu, H. B. Li, P. Tapponnier, B. Meyer, F. J. Ryerson, A. S. Meriaux, and Z. Q. Xu (2001), Rapid active thrusting along the northwestern range front of the Tanghe Nan Shan (western Gansu, China), *J. Geophys. Res.*, *106*, 30,475–30,504, doi:10.1029/2001JB000583.

Vincent, S. J., and M. B. Allen (1999), Evolution of the Minle and Chaoshui Basins, China: Implications for Mesozoic strike-slip basin formation in Central Asia, *Geol. Soc. Am. Bull.*, *111*, 725–742.

Wang, Y., W. D. Mooney, X. Yuan, and N. Okaya (2013), Crustal structure of the northeastern Tibetan Plateau from the Southern Tarim Basin to the Sichuan Basin, China, *Tectonophysics*, *584*, 191–208.

Wang, Z., and X. Yu (1995), The Late Carboniferous rugose corals from Shihuigou on the north margin of the Qaidam Basin, *Acta Geosci. Sin.*, *3*, 310–327.

Washburn, Z., J. R. Arrowsmith, S. L. Forman, E. Cowgill, X. F. Wang, Y. Q. Zhang, and Z. L. Chen (2001), Late Holocene earthquake history of the central Altyn Tagh fault, China, *Geology*, *29*, 1051–1054.

Wells, D. L., and K. J. Coppersmith (1994), New empirical relationships among magnitude, rupture length, rupture width, rupture area, and surface displacement, *Bull. Seismol. Soc. Am.*, *84*, 974–1002.

Woodcock, N. H. (1986), The role of strike-slip faults at plate boundaries, *Phil. Trans. R. Soc. A*, *317*, 13–29.
Wu, C., A. Yin, A. V. Zuza, J. Zhang, W. Liu, and L. Ding (2016), Pre-Cenozoic geologic history of the central and northern Tibetan Plateau and the role of Wilson cycles in constructing the Tethyan orogenic system, *Lithosphere*, *8*, 254–292.
Xiao, W. J., F. Windley, Y. Yong, Z. Yan, C. Yuan, C. Z. Liu, and J. L. Li (2009), Early Paleozoic to Devonian multiple-accretionary model for the Qilian Shan, NW China, *J. Asian Earth Sci.*, *35*, 323–333.
Xu, X., S. G. Song, L. Su, Z. X. Li, Y. L. Niu, and M. B. Allen (2015), The 600–580 Ma continental rift basalts in North Qilian Shan, northwest China: Links between the Qilian-Qaidam block and SE Australia, and the reconstruction of East Gondwana, *Precambrian Res.*, *257*, 47–64.
Xu, X. W., R. S. Yeats, and G. H. Yu (2010), Five short historical earthquake surface ruptures near the silk road, Gansu Province, China, *Bull. Seismol. Soc. Am.*, *100*, 541–561.
Ye, Z., R. Gao, Q. S. Li, H. S. Zhang, X. Z. Shen, X. Z. Liu, and C. Gong (2015), Seismic evidence for the North China plate underthrusting beneath northeastern Tibet and its implications for plateau growth, *Earth Planet. Sci. Lett.*, *426*, 109–117.
Yin, A., and T. M. Harrison (2000), Geologic evolution of the Himalayan-Tibetan orogen, *Annu. Rev. Earth Planet. Sci.*, *28*, 211–280.
Yin, A., Y. Q. Dang, L. C. Wang, W. M. Jiang, S. P. Zhou, X. H. Chen, G. E. Gehrels, and M. W. McRivette (2008a), Cenozoic tectonic evolution of Qaidam basin and its surrounding regions (Part 1): The southern Qilian Shan-Nan Shan thrust belt and northern Qaidam basin, *Geol. Soc. Am. Bull.*, *120*, 813–846.
Yin, A., Y. Q. Dang, M. Zhang, X. H. Chen, and M. W. McRivette (2008b), Cenozoic tectonic evolution of the Qaidam basin and its surrounding regions (Part 3): Structural geology, sedimentation, and regional tectonic reconstruction, *Geol. Soc. Am. Bull.*, *120*, 847–876.
Yuan, D. Y., J.-D. Champagnac, W.-P. Ge, P. Molnar, P.-Z. Zhang, W.-J. Zheng, H.-P. Zhang, and X.-W. Liu (2011), Late Quaternary right-lateral slip rates of faults adjacent to the lake Qinghai, northeastern margin of the Tibetan Plateau, *Geol. Soc. Am. Bull.*, *123*, 2016–2030.
Yuan, D. Y., et al. (2013), The growth of northeastern Tibet and its relevance to large-scale continental geodynamics: A review of recent studies, *Tectonics*, *32*, 1358–1370, doi:10.1002/tect.20081.
Zhang, H. P., W. H. Craddock, R. O. Lease, W. T. Wang, D. Y. Yuan, P. Z. Zhang, P. Molnar, D. W. Zheng, and W. J. Zheng (2012), Magnetostratigraphy of the Neogene Chaka basin and its implications for mountain building processes in the north-eastern Tibetan Plateau, *Basin Res.*, *24*, 31–50.
Zhang, J. X., Z. M. Zhang, Z. Q. Xu, J. S. Yang, and J. W. Cui (2001), Petrology and geochronology of eclogites from the western segment of the Altyn Tagh, northwestern China, *Lithos*, *56*, 187–206.
Zhang, P. Z., Z. Shen, M. Wang, W. J. Gan, R. Burgmann, and P. Molnar (2004), Continuous deformation of the Tibetan Plateau from global positioning system data, *Geology*, *32*, 809–812.
Zhang, Z., R. McCaffrey, and P. Zhang (2013), Relative motion across the eastern Tibetan Plateau: Contributions from faulting, internal strain and rotation rates, *Tectonophysics*, *584*, 240–256.
Zheng, D. W., M. K. Clark, P. Z. Zhang, W. J. Zheng, and K. A. Farley (2010), Erosion, fault initiation and topographic growth of the North Qilian Shan (northern Tibetan Plateau), *Geosphere*, *6*, 937–941.
Zheng, W. J., P. Z. Zhang, W. P. Ge, P. Molnar, H. P. Zhang, D. Y. Yuan, and J. H. Liu (2013a), Late Quaternary slip rate of the South Heli Shan Fault (northern Hexi Corridor, NW China) and its implications for northeastward growth of the Tibetan Plateau, *Tectonics*, *32*, 271–293, doi:10.1002/tect.20022.
Zheng, W. J., P. Z. Zhang, W. G. He, D. Y. Yuan, Y. X. Shao, D. W. Zheng, W. P. Ge, and W. Min (2013b), Transformation of displacement between strike-slip and crustal shortening in the northern margin of the Tibetan Plateau: Evidence from decadal GPS measurements and late quaternary slip rates on faults, *Tectonophysics*, *584*, 267–280.
Zhuang, G., J. K. Hourigan, B. D. Ritts, and M. L. Kent-Corson (2011), Cenozoic multiple-phase tectonic evolution of the northern Tibetan Plateau: Constraints from sedimentary records from Qaidam Basin, Hexi Corridor, and Subei Basin, Northwest China, *Am. J. Sci.*, *311*, 116–152.
Zuza, A. V., and A. Yin (2016), Continental deformation accommodated by non-rigid passive bookshelf faulting: An example from the Cenozoic tectonic development of northern Tibet, *Tectonophysics*, *677*, 227–240.
Zuza, A. V., X. Cheng, and A. Yin (2016), Testing models of Tibetan Plateau formation with Cenozoic shortening estimates across the Qilian Shan-Nan Shan thrust belt, *Geosphere*, *12*, 501–532.